Photoacoustic imaging of biological tissue with intensity-modulated continuous-wave laser

Konstantin Maslov
Lihong V. Wang
Washington University in St. Louis
Department of Biomedical Engineering
Optical Imaging Laboratory
Campus Box 1097, One Brookings Drive
St. Louis, Missouri 63130-4899

Abstract. We build a photoacoustic imaging system using an intensity-modulated continuous-wave laser source, which is an inexpensive, compact, and durable 120-mW laser diode. The goal is to significantly reduce the costs and sizes of photoacoustic imaging systems. By using a bowl-shaped piezoelectric transducer, whose numerical aperture is 0.85 and resonance frequency is 2.45 MHz, we image biological tissues with a lateral resolution of 0.45 mm, an axial resolution of 1 mm, and an SNR as high as 43 dB. © *2008 Society of Photo-Optical Instrumentation Engineers.* [DOI: 10.1117/1.2904965]

1 Introduction

Photoacoustic (PA) imaging[1–8] is a hybrid technology that maps the internal distribution of optical energy deposition (specific absorption) in biological tissues by detecting laser-induced ultrasonic (so-called PA) waves. PA imaging takes advantage of the weaker ultrasonic scattering, whose magnitude per unit path length is two orders of magnitude less than that of optical scattering,[9] to combine ultrasonic resolution with optical contrast. PA imaging is able to extract certain physiological parameters for functional imaging by varying the optical wavelength of the excitation laser.[10]

State-of-the-art PA techniques always use pulsed lasers as the PA excitation source. The major reasons for this choice include (1) high energy in each laser pulse—even if within the ANSI safety limit[11]—yields strong PA signals, leading to a good signal-to-noise ratio[12] (SNR), (2) PA transients provide axial resolution along the ultrasonic propagation direction, and (3) difference in the time of flight of PA waves reduces signal cluttering. For example, the first dark-field confocal PA microscope (PAM) using pulsed laser illumination is capable[13] of imaging biological tissue with ~15 μm axial resolution, 45 to 120 μm lateral resolution, and ~40 dB SNR. Pulsed PA imaging techniques, however, suffer from laser jittering as well as acoustic and thermal noises within the wide bandwidth of the ultrasonic transducer. In addition, high-energy pulsed lasers are expensive and bulky, which limits the applications of PA imaging technologies in medicine and biology.

Continuous-wave (cw) PA excitation sources such as high-power laser diodes,[14] which are inexpensive, compact, and durable, offer attractive alternatives. A cw PA detection with a narrow-band ultrasonic transducer and a narrow-band or lock-in amplifier provides high sensitivity and strong noise rejection. A cw PAM based on lock-in detection has been demonstrated to measure surface[15] and subsurface[16] properties of solids. Although single-frequency detection does not enable unequivocal phase-based axial resolution owing to the 2π phase ambiguity, chirping (frequency sweeping) over a bandwidth enables full axial resolution, which is comparable to the time-domain resolution acquired with the same bandwidth. However, single-frequency detection with a focused ultrasonic transducer can provide amplitude-based axial resolution as will be shown later. In addition, dual-frequency detection can be tailored to reject undesirable PA signals from a particular depth.

In this study, we investigated the possibility of cw PA imaging of biological tissue using a laser diode as a PA source. We also compared the sensitivity of the cw technique with the pulsed counterpart.[10]

2 Theory

Because laser diodes produce peak powers several orders of magnitude less than Q-switched lasers, special attention should be paid to the SNR. We first consider the peak PA pressure generated by light absorption. In the case of pulsed excitation, the light intensity can be approximated by a Gaussian function: $I \approx E_P(\omega_P/\tau\sqrt{\pi}) \exp(-t^2/\tau^2)$, where E_P is the optical fluence, and τ is the pulse width ($\omega_P \approx 1/\tau$ is the cut-off frequency of the PA transient). In the case of intensity-modulated cw excitation, the light intensity is given by $I = I_{cw}[1 + \sin(\omega_c t)]$, where I_{cw} is the time-averaged light intensity, and ω_c is the modulation frequency. If light intensity is expressed as $I = I_0 f(\hat{t})$, where I_0 denotes the maximum, and $\hat{t}$ denotes a dimensionless time ($\hat{t} = t/\tau$ or $\omega_c t$), the associated

Address all correspondence to Lihong Wang, Biomedical Engineering, Washington University in St. Louis, One Brooking Drive, Campus Box 1097, St. Louis, Missouri 63130; Tel: (314)935–6152; Fax: (314)935–7448; E-mail: lhwang@biomed.wustl.edu

PA pressure is proportional[17] to $df(\hat{t})/d\hat{t}$. Consequently, regardless of the absorber geometry,[18] the maximum PA pressure due to pulsed excitation is given by $p_{P,\max} \propto (2/\pi e)^{1/2} E_P \omega_P$, whereas the PA pressure amplitude due to cw excitation is given by $p_{cw,\max} \propto I_{cw}$.

In both the pulsed and cw modes, the maximum values of E_P and I_{cw} are limited by the ANSI safety standards.[11] In the visible spectral region, the maximum E_P is 20 mJ/cm^2 and the maximum I_{cw} is 200 mW/cm^2. To achieve comparable lateral resolution between the pulsed and cw modes, we assume $\omega_P = \omega_c$. If $\omega_c/2\pi$ is set to 2.45 MHz, we find that $p_{P,\max}$ is approximately six orders of magnitude (120 dB) stronger than $p_{cw,\max}$.

The difference in bandwidth between the two modes offsets the difference in signal strength because noise amplitude is proportional to the square root of the signal bandwidth. In pulsed mode, the cutoff frequency of the bandwidth is $\Delta f_P \propto \omega_P/2\pi$. In cw mode, the bandwidth is limited only by the desired data acquisition rate of each pixel of the image, which can be set to the 10-Hz laser repetition rate of the table-top PAM system under comparison. This difference in bandwidth increases the ratio of the SNR of the cw mode to that of the pulsed mode by approximately three orders of magnitude (60 dB).

The difference in sensitivity between the ultrasonic transducers used in the two modes further offsets the difference in signal strength. In pulsed mode, the piezoelectric transducer, which must have a broad bandwidth, typically has an insertion loss[19] of the order of 20 dB. This loss is due to either the low electromechanical coupling coefficient K of piezoelectric material or the high acoustic impedance Z because no piezoelectric material can yet provide both high K and low Z. For example, polymers such as PVDF have low Z but also low K, whereas piezoceramics such as PZT have high K but also high Z. High Z ultrasonic transducers present strong acoustic impedance mismatch with soft biological tissue, which causes strong acoustic reflection at the interface. In cw mode, a low-loss resonant piezoelectric transducer can be used. When the thickness of the piezoelectric material equals one half of the acoustic wavelength, acoustic reflection at the interface in theory approaches zero. As a result, resonant transducers can be made of high K and high Z piezoceramic materials. In addition, resonant transducers are not required to use damping backing material, which is acoustically lossy. Therefore, a resonant transducer suffers from only electrical resistive loss and mechanical loss in the piezoelectric material. At a few megahertz frequency, these losses can be as little as a few decibels. In the end, this difference translates into approximately another order of magnitude (20 dB) improvement in SNR for cw detection.

The difference in signal strength can also be offset by using higher intensity laser diodes that are modulated with low duty cycle tone bursts. According to the ANSI standards[11] for less than 10 s of exposure, the maximum permissible exposure is limited by $1100 t_e^{1/4}$ in millijouls per square centimeter, where t_e denotes the exposure duration in seconds. For a 10-Hz pulse repetition frequency with a 1% duty cycle, the maximum permissible exposure is 20 W/cm^2, at which the SNR can be improved by another order of magnitude (20 dB).
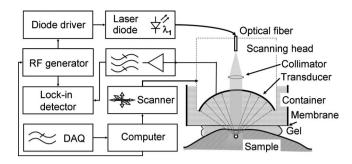

Fig. 1 Schematic of the cw PA imaging system.

Altogether the aforementioned three factors can offset the difference in signal strength between pulsed and cw modes by approximately five orders of magnitude. Therefore, a fully implemented cw system should provide a SNR about only one order of magnitude (20 dB) worse than that of a pulsed system. We so far, however, have taken advantage of only the first two factors. As a result, the SNR of the cw system is expected to be about two orders of magnitude (40 dB) worse than that of a pulse system.

3 Instrumentation

The pulsed-laser-based PAM system is similar to the high-frequency (50-MHz) version described elsewhere.[10,13] A tunable dye laser (ND6000, Continuum, California) pumped by an Nd:YAG laser (Brilliant B, Bigsky, Montana; pulse duration, 6.5 ns; repetition rate, 10 Hz) serves as the PA excitation source. The pulsed system uses a 5-MHz spherically focused ultrasonic transducer made of composite material (113-842-320, GE Inspection Technology; diameter, 6.35 mm; focal length, 18 mm). The incident fluence on the sample surface and at the optical focus is[11] <20 mJ/cm^2 (the ANSI safety limit). To acquire an image, the PAM system records the PA wave at each location of the ultrasonic transducer and performs raster-scanning in the horizontal ($x-y$) plane with a step size of 125 μm.

The cw PA imaging system uses a scanning system similar to the one in the pulsed PAM system but different optical excitation and data acquisition systems (see Fig. 1). An inexpensive, compact, and durable laser diode (GH0781JA2C, Sharp; power: 120 mW; wavelength: 784 nm) driven by a laser diode current controller (LDC220, Thorlabs) is the excitation source. We modulate the power of the laser diode at 2.45 MHz with a 100% modulation depth by applying a 10-V sinusoidal signal from a function generator to the laser bias through a serial 50 Ω resistor. Light from the laser diode is delivered via an optical fiber. The transmitted light passes to the sample through a 5-mm-diam optical collimating lens secured within the hole on the axis of the transducer. The resulting time-averaged spatial peak optical power density on the sample surface after loss in the light delivery system was measured to be near but within ANSI safety limit of 200 mW/cm^2. An ultrasonic transducer has a bowl-shaped piezoceramic active element (Pz27 ceramic, Ferroperm Piezoceramics A/S, Kvistgaard, Denmark) with a 38 mm diameter and a 22 mm radius of curvature. The through-thickness resonance frequency of the transducer is 2.45 MHz. Gold elec-

trodes are deposited on the two spherical surfaces of the active element. The electrode on the concave spherical surface is soldered to the transducer shell with low-melting-point alloy (SnCuInCd eutectic), whereas the other electrode is connected to a resonant preamplifier via an impedance-matching line transformer. The preamplified PA signal is detected by a lock-in amplifier (SR844, Stanford Research Systems), which is used as both a phase-sensitive detector and a data acquisition system. The components within the dashed-box in Fig. 1 are translated within a container with immersion liquid (water). A window at the bottom of the water container is sealed with an optically and ultrasonically transparent polyethylene membrane (thickness, 0.044 mm). During data acquisition (DAQ), a sample is placed below the membrane and acoustically coupled with commercial ultrasound gel. The amplitude and phase of the signal are analyzed by a laptop computer, which also controls the mechanical scanner.

4 Animal Protocol

New Zealand white rabbits with body weights between 2.8 and 3.5 kg were used for the experiments. Immediately after the rabbits were sacrificed by an overdose of pentobarbital, the ears and legs were removed. Wounds were sealed with surgical glue (NEXABAND, Closure Medical Corporation, North Carolina). Hairs were shaved off with a veterinary shaving device. The tissue was placed on top of a 10-mm layer of acoustic impedance-matching rubber, which absorbs transmitted ultrasound. The tissue was then imaged by the cw PA imaging system. The samples were also photographed. All experimental animal procedures were carried out in conformity with the guidelines of the National Institutes of Health[20] (NIH). The laboratory animal protocol for this work was approved by the School of Medicine Animal Studies Committee of Washington University at Saint Louis.

5 Results and Discussion

The lower bound of the SNR is estimated by imaging an edge of a highly optically absorptive black polyethylene film in water using the cw PA imaging system. The image contrast is found to be ~43 dB, which can also be interpreted as the lower bound of the SNR. A similar experiment is conducted using the pulsed system, the image contrast is found to be ~77 dB. Therefore, the pulsed system yields a 34 dB greater SNR than the cw system. This difference agrees with the aforementioned theoretical expectation.

The lateral resolution of the cw system is tested by imaging a 60-μm-diam human hair immersed in a 0.2% Intralipid® solution. The hair is oriented along the Y axis, which is normal to the transducer axis (Z). The PA signal amplitude is plotted as a function of the Z and X axes in Fig. 2, which is referred to as the line spread function. The lateral resolution is estimated to be ~450 μm, which is in good agreement with the theoretical prediction [0.61λ/numerical aperture (NA)=430 μm, where λ=600 μm is the acoustic wavelength and NA=0.85 is the NA of the spherical transducer]. The axial resolution at the −6-dB level is estimated to be ~1 mm, which matches approximately the 2 mm full width at half maximum of the pressure sensitivity distribution along the acoustic axis in the focal zone of the transducer. The
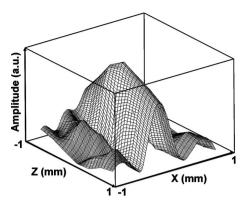

Fig. 2 Line spread function of the cw PA imaging system.

pressure sensitivity distribution can be computed[21] by $P(u) = P_0[\sin(u/4)/(u/4)]$, where P_0 is the peak pressure sensitivity and $u = (2\pi Z/\lambda)(\text{NA})$.

To demonstrate the feasibility of cw PA imaging for biomedical applications, we imaged vascular networks in rabbit ears.[22] An amplitude image—a plot of the PA signal amplitude versus the scanned positions of the ultrasonic transducer—of a rabbit ear is shown in Fig. 3(a), which shows the vasculature clearly. The scanning step size was 150 μm in both the X and Y directions. Raster scanning was performed with a scanning speed of 10 steps (pixels)/s, whereas the integration time of the lock-in amplifier was 30 ms. The rabbit ear was then transilluminated for photography of the vasculature [Figs. 3(b) and 3(c)]. The major arteries and veins were located between the central layer of cartilage and the dorsal skin. The skin overlying the imaged vasculature measured on average 300 μm in thickness. Figure 3(b) shows a close-up of the vascular anatomy within the PA scanning area, which displays small branches from the central auricular branch and tributaries from the rostral auricular vein. The smallest vessel visualized by the cw PA imaging system in this specific region of the ear has a diameter of approximately 200 μm, estimated from the photograph. There is good correspondence between the PA image and the photograph, although some artifacts are apparent. The artifacts are probably due to the interference between PA signals originating from different locations. In addition, ultrasonic reflections from the sample boundaries
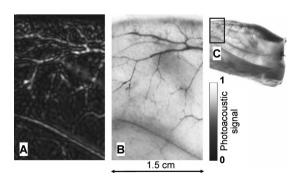

Fig. 3 (A) Amplitude image of a rabbit ear vasculature acquired with the cw PA imaging system, (B) photograph of the imaged region of the ear, and (C) photograph of the entire ear. The imaged region in (B) is marked with a frame.
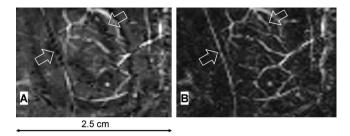
Fig. 4 Amplitude images of a rabbit ear vasculature acquired with the cw PA imaging system (A) before and (B) after removal of interference artifacts. Arrows indicate some much improved structures.

Fig. 5 (A) Amplitude image of a rabbit tibial artery (TA) and a tibial vein (TV) acquired with the cw PA imaging system and (B) photographs of the anatomical cross sections indicated by S1 and S2 in (A) through the leg muscle.

and the transducer surface as well as leakage of the laser-modulation electrical signal into the lock-in amplifier can also cause artifacts.

On the basis of the Fourier transform, the cw mode with the modulation frequency swept over a bandwidth is equivalent to the pulsed mode with the same bandwidth. Therefore, PA sources can be localized by sweeping the modulation frequency within the frequency band of the ultrasonic transducer.[15] In the frequency domain, the transducer output voltage $V(\omega)$ as a function of frequency ω is proportional to the PA pressure $p(\omega)$ multiplied by both the frequency response of the ultrasonic receiver and the phase shift due to the PA wave propagation distance z_0 from the PA source to the ultrasonic transducer. The frequency-dependent ultrasonic attenuation in the medium can be included as well. Here, we consider only a single small-sized PA source although the same principle applies to a distribution of PA sources. If the frequency response of the resonant transducer is assumed to have a Gaussian shape, we have

$$V(\omega) \propto p(\omega) \exp\left[-(\omega - \omega_0)^2/(\Delta\omega)^2\right] \exp\left(i\omega z_0/c\right). \quad (1)$$

By virtue of the Fourier transformation and the relation $z = ct$, Eq. (1) can be converted into the space domain:

$$V(z) \propto p(z) \otimes \exp\left\{-\left[\pi\frac{(z - z_0)}{\lambda}\frac{\Delta\omega}{\omega_0}\right]^2\right\}, \quad (2)$$

where λ denotes the wavelength of the PA wave at frequency ω_0 and $\otimes$ denotes convolution. We can see that the PA source is localized with a resolution related to the ultrasonic wavelength multiplied by a factor of $\omega_0/\pi\Delta\omega$. The resolution can be related to the pulse width in the time domain multiplied by the speed of sound. In practice, the system frequency response can be measured by recording the amplitude and phase of the transducer output in response to a small test target placed at the focal spot of the transducer, and the continuous Fourier transformation can be implemented in its discrete form. Since $\Delta\omega \ll \omega_0$ for a resonant transducer, frequency sweeping will not be broad enough to achieve high spatial resolution. If a broadband transducer is used instead, the sensitivity will be reduced.

In some cases, a few frequencies are sufficient to remove some most significant imaging artifacts. Some interference artifacts are indicated by arrows in Fig. 4(a). Here, we assume that the interference is between the PA signals from blood vessels and the front surface of the transducer. We use two
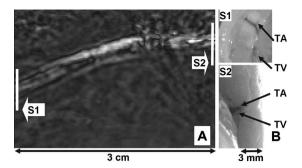
frequencies shifted by $\Delta f = c/2z_0$ and simply subtract the two transducer outputs. The difference image is shown in Fig. 4(b). As can be seen, this simple procedure significantly improves the image quality. For example, some blood vessels that show lengthwise contrast inversion in Fig. 4(a), as indicated by arrows, become uniformly bright in Fig. 4(b).

To demonstrate the capability of the cw system to image relatively deep structures, we further imaged a rabbit leg using the cw PA imaging system [Fig. 5(a)]. Two anatomical cross sections were photographed for comparison [Fig. 5(b)]. The bright structures shown in Fig. 5(a) are the TA and TV. The diameters of the TA and TV are both ~1 mm as estimated by optical microscopy. The scanning area covers 30 $\times$ 20 mm through 240 and 160 scanning steps in the X and Y directions, respectively. As revealed by Fig. 5(b), the main branches of both the tibial artery and tibial vein seat below a 2.4 to 3.4-mm-thick layer of skin and muscle tissue.

The current cw system has relatively long data acquisition time. If the data acquisition time per pixel is 90 ms, the scan time for a 10,000-pixel 2=D en face image using the current cw system can be as long as 15 min. If only a 100-pixel 1=D image is needed, the acquisition time is shortened to 9 s. Use of an ultrasound array can potentially speed up the data acquisition.

If depth resolution is not important in a particular application, cw imaging can serve as a viable alternative to pulsed mode imaging. Like pulsed PA imaging,[2,10] cw imaging can provide functional information of biological tissue as well if multiple laser diodes of different wavelengths are used for spectral measurements. Possible applications of the cw technique may include for example sentinel lymph node mapping[23] and cerebral blood oxygenation monitoring[24].

6 Conclusions

In this feasibility study, we demonstrated that the cw PA imaging technique can image blood vessels ~3 mm deep in tissue. The cw system was built using an intensity-modulated cw laser diode. As a result, the imaging system is inexpensive, compact, and durable. Although a single-frequency cw measurement cannot provide the time-domain information about the PA time of flight, a spherically focused acoustic lens can provide spatial resolution. Using a bowl-shaped piezoelectric transducer with an NA of 0.85 and a resonance frequency of

2.45 MHz, we imaged biological tissues with a lateral resolution of 450 μm, an axial resolution of 1 mm, and an SNR as high as 43 dB.

References

1. M. Xu, and L. V. Wang, "Photoacoustic imaging in biomedicine," *Rev. Sci. Instrum.* **77**, 041101 (2006).
2. X. Wang, Y. Pang, G. Ku, X. Xie, G. Stoica, and L. V. Wang, "Noninvasive laser-induced photoacoustic tomography for structural and functional imaging of the brain in vivo," *Nat. Biotechnol.* **21**, 803–806 (2003).
3. C. G. A. Hoelen, F. F. M. de Mul, R. Pongers, and A. Dekker, "Three-dimensional photoacoustic imaging of blood vessels in tissue," *Opt. Lett.* **23**, 648–650 (1998).
4. A. Oraevsky and A. Karabutov, "Optoacoustic tomography," in *Biomedical Photonics Handbook*, Vol. **PM125**, T. Vo-Dinh, Ed., CRC Press, Boca Raton, FL (2003).
5. R. A. Kruger, P. Liu, Y. R. Fang, and C. R. Appledorn, "Photoacoustic ultrasound (PAUS) reconstruction tomography," *Med. Phys.* **22**, 1605–1609 (1995).
6. A. G. Bell, "On the production and reproduction of sound by light," *Am. J. Sci.* **20**, 305–324 (1880).
7. G. J. Diebold, M. I. Khan, and S. M. Park, "Photoacoustic 'signature' of particulate matter: optical production of acoustic monopole radiation," *Science* **250**, 101–104 (1990).
8. A. C. Tam, "Applications of photoacoustic sensing techniques," *Rev. Mod. Phys.* **58**, 381–431 (1986).
9. F. A. Duck, *Physical Properties of Tissue*, Academic Press, London (1990).
10. H. F. Zhang, K. Maslov, G. Stoica, and L. V. Wang, "Functional photoacoustic microscopy for high-resolution and noninvasive in vivo imaging," *Nat. Biotechnol.* **24**, 848–851 (2006).
11. Laser Institute of America, *American National Standard for Safe Use of Lasers*, ANSI Z136.1-2000, American National Standards Institute, Inc., New York (2000).
12. A. Oraevsky and A. Karabutov, "Ultimate sensitivity of time-resolved optoacoustic detection, biomedical optoacoustics," *Proc. SPIE* **3916**, 228–239 (2000).
13. K. Maslov, G. Stoica, and L. V. Wang, "In vivo dark-field reflection-mode photoacoustic microscopy," *Opt. Lett.* **30**, 625–627 (2005).
14. T. J. Allen and P. C. Beard, "Pulsed near-infrared laser diode excitation system for biomedical photoacoustic imaging," *Opt. Lett.* **31**, 3462–3464 (2006).
15. T. W. Murray and O. Balogun, "High-sensitivity laser-based acoustic microscopy using a modulated excitation source," *Appl. Phys. Lett.* **85**, 2974–2476 (2004).
16. Y. Fan, A. Mandelis, G. Spirou, and I. A. Vitkin, "Development of a laser photothermoacoustic frequency-swept system for subsurface imaging: theory and experiment," *J. Acoust. Soc. Am.* **116**, 3523–3533 (2004).
17. I. G. Calasso, W. Craig, and G. J. Diebold, "Photoacoustic point source," *Phys. Rev. Lett.* **86**, 3550–3553 (2001).
18. G. J. Diebold, T. Sun, and M. I. Khan, "Photoacoustic monopole radiation in one, two, and three dimensions," *Phys. Rev. Lett.* **69**, 3384–3387 (1991).
19. M. Robert, G. Molingou, and K. Snook, "Fabrication of focused polyvinylidene fluoride-trifluoroethylene PVDF-TrFE copolymer 40–50 MHz ultrasound transducers on curved surfaces," *J. Appl. Phys.* **96**, 252–257 (2004).
20. National Institutes of Health, *Guide for the Care and Use of Laboratory Animals*, NIH Pub. 86-23, U.S. Government Printing Office, Washington, DC (1985).
21. M. Born and E. Wolf, *Principles of Optics: Electromagnetic Theory of Propagation, Interference and Diffraction of Light*, 5th ed., p. 436 (Pergamon Press, Oxford, 1975).
22. R. I. Siphanto, R. G. Kolkman, A. Huisjes, M. C. Pilatou, F. F. de Mul, W. Steenbergen, and L. N. van Adrichem, "Imaging of small vessels using photoacoustics: an in vivo study," *Lasers Surg. Med.* **35**, 354–362 (2004).
23. A. Darzi and S. Mackay, "Recent advances in minimal access surgery," *Br. Med. J.* **324**, 31–34 (2002).
24. Y. Y. Petrov, D. S. Prough, D. J. Deyo, M. Klasing, M. Motamedi, and R. O. Esenaliev, "Optoacoustic, noninvasive, real-time, continuous monitoring of cerebral blood oxygenation: an in vivo study in sheep," *Anesthesiology* **102**, 69–75 (2005).